

Quasi-Monolayer Black Phosphorus with High Mobility and Air Stability

Sherman Jun Rong Tan, Ibrahim Abdelwahab, Leiqiang Chu, Sock Mui Poh, Yanpeng Liu, Jiong Lu, Wei Chen, and Kian Ping Loh*

Black phosphorus (BP) exhibits thickness-dependent band gap and high electronic mobility. The chemical intercalation of BP with alkali metal has attracted attention recently due to the generation of universal superconductivity regardless of the type of alkali metals. However, both ultrathin BP, as well as alkali metal-intercalated BP, are highly unstable and corrode rapidly under ambient conditions. This study demonstrates that alkali metal hydride intercalation decouples monolayer to few layers BP from the bulk BP, allowing an optical gap of ≈ 1.7 eV and an electronic gap of 1.98 eV to be measured by photoluminescence and electron energy loss spectroscopy at the intercalated regions. Raman and transport measurements confirm that chemically intercalated BP exhibits enhanced stability, while maintaining a high hole mobility of up to ≈ 800 cm² V⁻¹ s⁻¹ and on/off ratio exceeding 10³. The use of alkali metal hydrides as intercalants should be applicable to a wide range of layered 2D materials and pave the way for generating highly stable, quasi-monolayer 2D materials.

Black phosphorus (BP) is the most stable allotrope of elemental phosphorus^[1] consisting of puckered P atom layers^[2] possessing highly anisotropic properties.^[3] Alkali metal intercalated BP has recently received considerable attention due to the ability to tune intrinsic p-doped BP to the n-doping regime^[4] as well as to convert BP into a Dirac semimetal.^[5] Additionally, alkali metal intercalated BP exhibits superconductivity with critical temperature > 3 K.^[6] The direct band gap, robust excitons, and quasi-1D trions in monolayer BP are highly attractive

for next-generation optical applications.^[7,8] Alkali metal intercalation can be applied to electronically decouple adjacent layers in 2D materials.^[9] Due to the low diffusion barrier along the zigzag direction at room temperature, BP exhibits highly anisotropic and fast alkali metal diffusion, which allows fast charge and discharge of ions during energy storage.^[4] However, alkali metal intercalated BP is highly unstable due to oxidation process in the presence of light, water, and oxygen.^[10,11]

Recent passivation approaches to stabilize BP flakes include coating with Al₂O₃ using atomic layer deposition,^[12,13] encapsulation by hexagonal boron nitride (h-BN),^[14] oxygen plasma etching followed by Al₂O₃ coating,^[15] and covalent functionalization.^[10] However, some of these methods are incompatible with the intercalated alkali metal due to side reactions.

Furthermore, plasma etching and covalent functionalization inevitably introduce undesirable and irreversible defects and modifications to BP, resulting in poor device performance.^[16] Therefore, there is a need to identify a method to generate chemically stable, alkali-metal intercalated BP, such that the stability of such devices can be sufficiently enhanced for applications in nanoelectronics, energy storage, and optoelectronics.


Herein, we intercalated BP with LiH (abbreviated as LiH-BP), this has the effect of converting bulk BP into highly stable, quasi-monolayer BP, which provides a stark contrast to air-exposed, exfoliated BP which degrades rapidly within hours. LiH-BP exhibits photoluminescence (PL) consistent with the optical gap of monolayer BP, which indicates that the intercalation of a bulk BP crystal decouples the near surface region into quasi-monolayer BP. Surface analysis using X-ray photoemission spectroscopy (XPS) reveals that LiH intercalation reduces the oxygen reactivity of BP. Low energy electron diffraction (LEED) reveals that LiH-BP retains good crystallinity and transport study shows that it has carrier mobility up to ≈ 800 cm² V⁻¹ s⁻¹ even after ambient exposure. Our study therefore demonstrates a way to prepare air stable, quasi-monolayer BP on bulk BP without mechanical exfoliation, and opens up possibilities for investigating the novel electronic and optoelectronic properties of highly unstable layered 2D systems which are difficult to exfoliate.

Black Phosphorus is a 2D layered material held by van der Waal's interactions as shown in **Figure 1**. The spaces between the layers allow for the intercalation of alkali metals; however,

S. J. R. Tan, I. Abdelwahab, Dr. L. Chu, S. M. Poh, Dr. Y. Liu,
Prof. J. Lu, Prof. W. Chen, Prof. K. P. Loh
Department of Chemistry
National University of Singapore
Singapore 117543, Singapore
E-mail: chmlhkp@nus.edu.sg

S. J. R. Tan, I. Abdelwahab, S. M. Poh
NUS Graduate School for Integrative Sciences and Engineering
National University of Singapore
Centre for Life Sciences
#05-01, 28 Medical Drive, Singapore 117456, Singapore

Prof. K. P. Loh
Centre for Advanced 2D Materials and Graphene Research Centre
National University of Singapore
Singapore 117546, Singapore

 The ORCID identification number(s) for the author(s) of this article can be found under <https://doi.org/10.1002/adma.201704619>.

DOI: 10.1002/adma.201704619

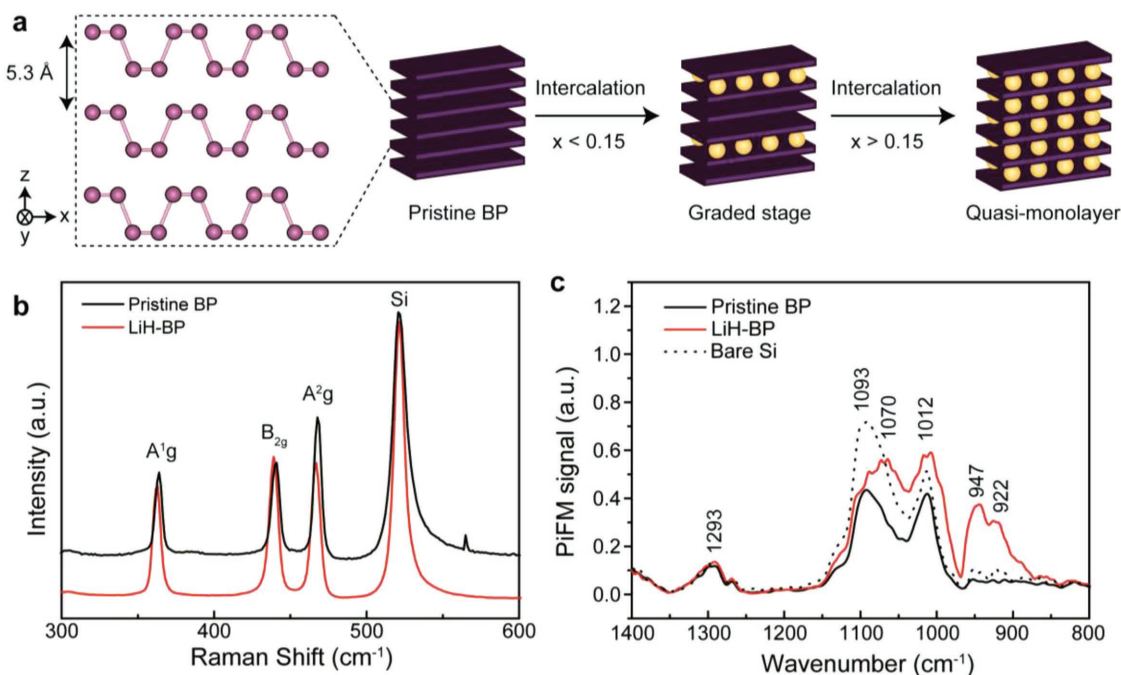


Figure 1. a) Schematic showing LiH-intercalated BP showing few-layer ($x < 0.15$) and monolayer ($x > 0.15$) intercalated stage, where x refers to the atomic ratio of Li. Zoomed in side view model of black phosphorus is shown on the left. b) Raman spectrum of LiH-BP flake taken with 532 nm laser. Raman of pristine BP is shown for comparison. c) Infrared photoinduced force microscopy (IR PiFM) spectra of pristine BP and LiH-BP, showing the presence of LiH-related vibrational modes at 922 and 947 cm^{-1} in LiH-BP.

it is known that alkali metal vapor corrodes BP. A liquid phase intercalation approach using electride salt (lithium in liquid ammonia) has been applied previously for Li intercalation, but the handling of these chemicals is highly tedious.^[6] We found that Li evaporated from a standard Società Apparecchi Elettrotecniche Scientifici (SAES) getter source provides a convenient and corrosion-free way of intercalating BP at room temperature. The intercalated Li can be converted to LiH by in situ hydrogenation.^[17] As illustrated in Figure 1a, LiH intercalation of BP follows a two-stage process, the final product is a stable quasi-monolayer LiH-BP. Figure 1b shows the typical Raman spectrum of LiH-BP on 285 nm thick SiO_2 substrate taken with a 532 nm laser. The observed Raman peaks at 362, 438, and 466 cm^{-1} agree with the characteristic A^1g , B_{2g} , and A^2g modes of BP, respectively.^[17] In addition, there is a general redshift of the main Raman modes of BP (Figure S1, Supporting Information), which may be due to intercalation-induced uniaxial strain along the zigzag directions, as well as electron transfer effects commonly observed in 2D materials.^[18] Additionally, we note that the unique anisotropy of BP is retained (Figure S2, Supporting Information). The presence of LiH can be tracked using infrared photoinduced force microscopy (IR PiFM) with mid IR laser excitation. As shown in Figure 1c, two new peaks with energies of 922 and 947 cm^{-1} are present in the LiH-BP spectrum but not in pristine BP spectrum (and bare Si). These peaks are assigned to the transverse optical (TO) and longitudinal optical (LO) modes of LiH, respectively.^[19] The splitting of LO–TO modes is smaller than unintercalated LiH, which can be attributed to the decreased ionic character.^[20]

The intercalation process was monitored in situ by electron spectroscopic techniques. Angle-resolved X-ray photoemission

spectroscopy with a probe depth of ≈ 6 layers of BP shows constant Li:P XPS peak ratios within different escape depths of the photoemitted electrons (changing polar angles from 0° to 70°), indicating that Li is intercalated homogeneously within BP to a depth of ≈ 3 nm (Figure S3, Supporting Information). High resolution electron energy loss spectroscopy (HREELS) provides a continuous spectrum of all electronic excitations, in which the band gap of the sample can be extracted from a sharp core level onset delineated by an enhanced intensity from the background.^[21] An incident electron beam energy of 16 eV was chosen to minimize broadening of the energy onset due to Cherenkov radiation. The energy resolution can be obtained from the full-width at half maximum (FWHM) of the elastic peak and is determined to be 20 meV for pristine BP and 30 meV for LiH-BP. The emergence of peaks due to band-to-band electronic transitions in intercalated BP following the intercalation of LiH is shown in Figure 2. The spectra are normalized to the elastic peak of pristine BP, and the loss regions were scanned at the specular angle in the armchair direction. The loss region spectrum for pristine BP shows a single peak “P1” (onset energy = 0.31 eV) which we assign to the electronic band gap of bulk BP, in agreement with an earlier scanning tunneling spectroscopy study.^[22] Upon LiH intercalation, new broad peaks labeled as “P2” (onset energy = 0.84 eV) and “P3” (onset energy = 1.21 eV) emerge, which correspond to the band gaps of 2 layer and 3 layer BP, respectively.^[23] Upon further LiH intercalation, a new peak “P4” (onset energy = 1.98 eV) emerges, which agrees well with the direct band gap electronic transition of monolayer BP.^[24,25] The Lorentzian peaks at 0.72 and 0.88 eV can be assigned to trion and excitonic transitions (trion binding energy 0.16 eV), respectively.^[26]

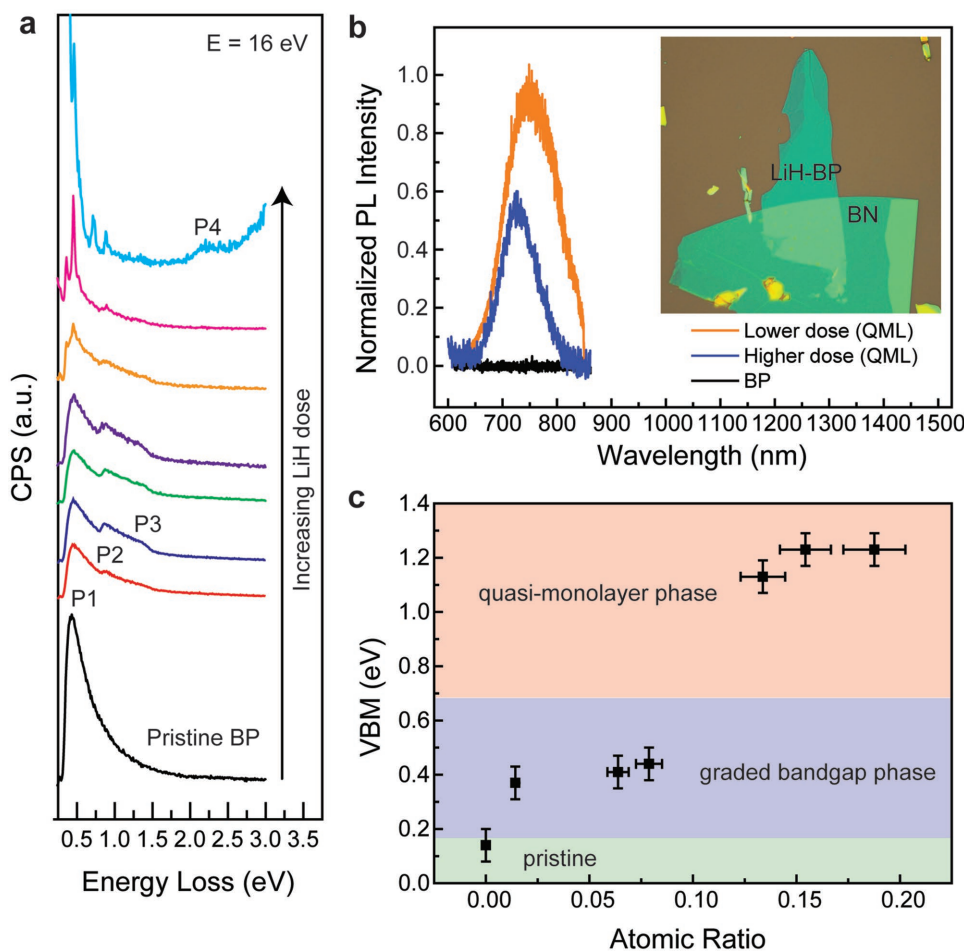


Figure 2. Intercalation-induced phase changes of BP. a) High resolution electron energy loss spectroscopy (HREELS) spectra of BP with increasing LiH dose. Spectra are normalized to the elastic peak of pristine BP (black) and the loss regions are magnified 100 times for clarity. b) Photoluminescence spectra of BP (BN covered) and LiH-BP (quasi-monolayer phase abbreviated QML) showing optical PL emission at ≈ 1.7 eV, corresponding to the optical band gap of monolayer phosphorene. c) Valence band maximum (VBM) shift of LiH-BP obtained from ultraviolet photoemission spectroscopy (UPS) as a function of atomic ratio of LiH obtained from X-ray photoemission spectroscopy (XPS). Atomic ratio of Li is determined by the relative XPS intensity ratios of Li to BP after correcting for their respective atomic sensitivity factors.

To confirm that quasi-monolayer BP was formed on bulk BP after Li intercalation, we probed the optical band gap of LiH-BP using PL. To compare LiH-BP with pristine BP, we cover half the BP flake with h-BN to block the intercalation, thus allowing only the exposed half to be intercalated (Figure 2b). The atomic force microscopy (AFM) image of this structure is shown in Figure S4 (Supporting Information), it should be pointed out that the flake height is 4.7 nm, far exceeding the thickness of monolayer BP (0.53 nm), thus any PL observed originates mainly from near surface regions which have been decoupled by Li intercalation. Indeed, PL emission at 729 and 748 nm (1.70 and 1.65 eV, respectively) can only be detected from the exposed flakes that were Li-intercalated, as shown in Figure 2b. The energy of PL emission agrees with what was reported previously for monolayer BP.^[15] The intensity of the PL is inversely proportional to the dose level, possibly due to PL quenching effect by the intercalants. By contrast, BN-covered, pristine BP does not exhibit any PL in the visible range; this is expected since pristine BP retains bulk behavior and emits in the infrared range. The exciton

binding energy can be estimated by taking the difference between the PL energy and the single particle gap determined by HREELS, from which a value of ≈ 0.28 eV is determined. Our measured value is smaller than the previously reported exciton binding energy of 0.90 eV for freestanding monolayer BP,^[25] the reasons could be due to screening effects from the underlying bulk BP substrate and the intercalants.

Additionally, we probed the evolution of valence band energy levels using ultraviolet photoemission spectroscopy (UPS), as shown in Figure S5 (Supporting Information). The evolution of valence band maximum (VBM) is correlated with the atomic ratio of LiH deposited (determined by XPS at a Li deposition rate of 0.31 ML h^{-1}) and is plotted in Figure 2c. Similar to our HREELS result, we observe the emergence of two new distinct phases, characterized by markedly different VBMs. For conventional doping-induced VBM shift, the rigid band model applies and the VBM shifts monotonically with the atomic ratio of the intercalant. However, in the case of LiH-BP, the VBM in each phase remains relatively constant, which may be pinned by electron traps present in the BP. It has been reported that

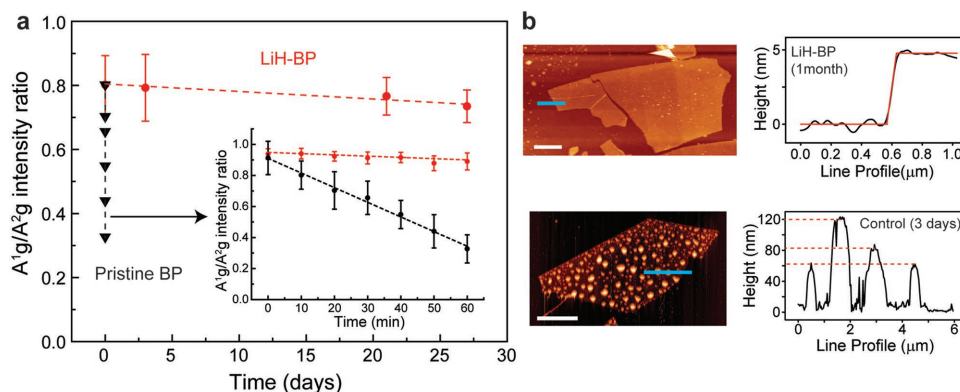


Figure 3. Stability study of BP and LiH-BP. a) Time evolution of integrated Raman peak ratio A^1g/A^2g of LiH-BP flake and pristine BP following exposure to air; the superior stability of LiH-BP is evident. Inset in (a) shows the magnified changes of the same in minutes scale. b) AFM investigation of surface morphology changes of LiH-BP (top panels) and BP treated with hydrogenation only (bottom panels) when subjected to ambient exposure. Left panels show the AFM topography and right panels show the line profile of the topography marked by a blue dash. Scale bar is $1 \mu\text{m}$ for top image and $5 \mu\text{m}$ for bottom image.

pristine BP contains a high concentration of electron trapping sites.^[27] When the atomic ratio (x) is larger than 0.15, the VBM increases abruptly to $\approx 1.23 \text{ eV}$; this implies that the band gap $> 1.23 \text{ eV}$, which suggests that quasi-monolayer phase has been formed at this stage. Our results show that the phase space of BP between different intercalation stages can be carefully controlled by the intercalation of LiH, which enables the band gap to be precisely controlled.

It is widely known that BP becomes more reactive as it is thinned down to the monolayer due to the shifts in band edge position, which has a stronger overlap with oxygen acceptor states.^[28] As such, it is especially challenging to obtain pristine monolayer BP in the ambient. We have evaluated the stability of quasi-monolayer LiH-BP by subjecting it to ambient exposure without any extra polymer encapsulation, and tracked structural degradation using Raman and AFM, as shown in **Figure 3**. The ratio of A^1g to A^2g Raman peak intensity is polarization insensitive and has been found to be a sensitive marker of the oxidative degradation of BP.^[28] Figure 3a shows the time evolution of the integrated peak ratio A^1g/A^2g of BP and LiH-BP. Additional stability testing based on intensity changes of Raman signals can be found in Figure S5 (Supporting Information). When the samples are prepared freshly, both pristine BP and LiH-BP have an initial A^1g/A^2g ratio of ≈ 0.8 . However, the A^1g/A^2g ratio decreases sharply for pristine BP after one day of exposure in the ambient, a key indication of oxidative degradation. By contrast, the A^1g/A^2g peak ratio of LiH-BP remains above 0.7 even after almost a month of air exposure. The slow decrease of A^1g/A^2g peak ratio observed for LiH-BP implies slow degradation in air, which is important for applications of alkali metal-intercalated BP under ambient conditions.

AFM provides a direct way to visualize ambient degradation of BP, which usually manifests in the form of surface protrusions due to the formation of phosphoric acid when BP is oxidized. It has been reported that small bumps ($\approx 2.5 \text{ nm}$) appearing on the surface of BP just after the exfoliation in air are indicative of oxidative degradation,^[13,29] and these will evolve into larger phosphoric acid droplets ($> 20 \text{ nm}$)^[28] after a few days. As shown in Figure 3b, no protrusions were observed

on LiH-BP even after ambient exposure for a month, as evidenced by the low surface roughness in the line profile. The small increase in substrate roughness was due to the oxidation of adsorbed Li on the substrate surface (Figure S6, Supporting Information). Notably, the apparent thickness of the LiH-BP flake had increased from ≈ 4 to $\approx 5 \text{ nm}$ as compared to the as-exfoliated flake, which could be ascribed to LiH intercalation. Our control experiment showed that hydrogenation (hydrogen passivation) of BP alone did not impart stability against degradation in air. Asperites $> 60 \text{ nm}$ appeared in the hydrogenated BP flakes (without Li intercalation) just after 3 days of ambient exposure as shown in Figure 3b. We also excluded possibility of stabilization due to Li-intercalation alone, and proved unequivocally that a two-step process, involving intercalation and hydrogenation of the alkali metal, was required to fully stabilize the intercalated phase.

To understand the origin of the air stability of quasi-monolayer LiH-BP, XPS studies were carried out to analyze the chemical phases on BP following various treatments, as shown in **Figure 4**. Pristine BP sample which was prepared by exfoliation in glove box and vacuum box-transferred to XPS system exhibits the spin-orbit doublet P $2p_{1/2}$ and P $2p_{3/2}$ core level peaks with binding energies of 131.2 and 130.2 eV, respectively. These peaks correspond to phosphorus-phosphorus bonds in BP, in agreement with earlier studies.^[30] Oxidized phosphorus species have binding energies higher than 134 eV, their absence in the XPS spectrum confirms the pristine quality of our exfoliated BP samples, which is further supported by their sharp LEED spots shown in the inset. After LiH intercalation, the P $2p_{3/2}$ core level peak shifts toward higher energy by 0.15 eV, due to n-doping induced Fermi level shift. Air exposure of LiH-BP causes the P $2p_{1/2}$ and P $2p_{3/2}$ core level peaks to be chemically shifted to 133.9 and 132.9 eV, respectively, as shown in Figure 4d, which we assigned to the formation of a metastable P_4O_2 phase.^[30,31] For comparison, when unhydrogenated LiBP was exposed to air, higher oxidation states P $2p_{1/2}$ and P $2p_{3/2}$ core level peaks at 136.2 and 135.2 eV, respectively, appeared due to the formation of P_2O_5 phase, as shown in Figure 4c. P_2O_5 phase also appeared for air-exposed pristine BP

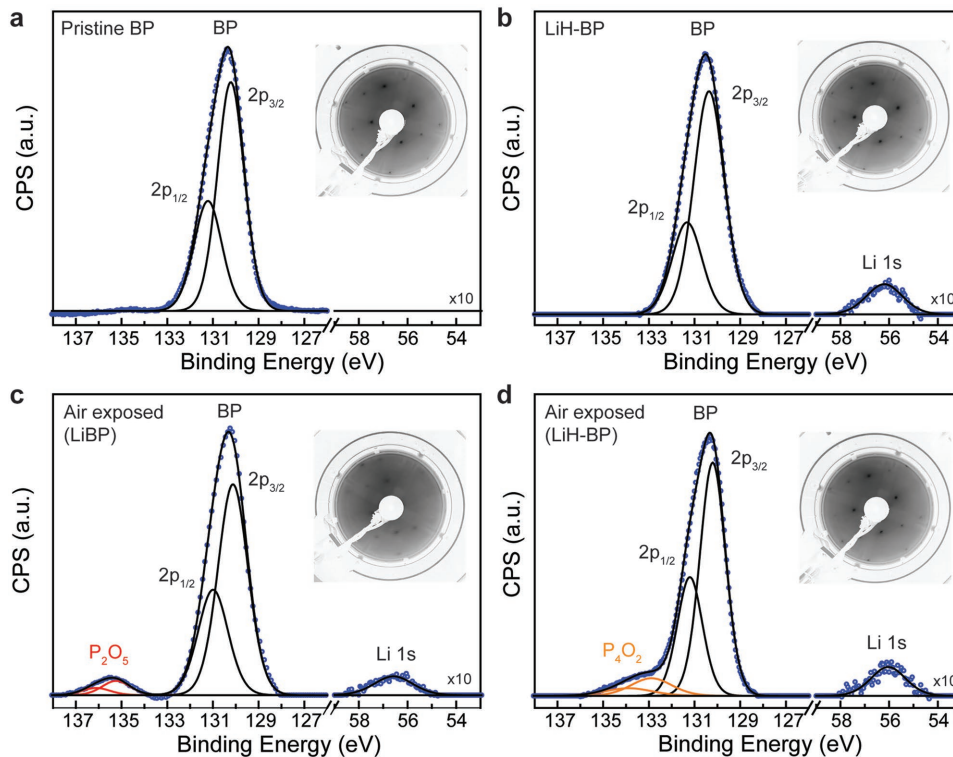


Figure 4. X-ray photoelectron Spectroscopy (XPS) characterizations of BP and LiH-BP. XPS spectra of a) pristine BP (a) and b) LiH-BP showing the P 2p and Li 1s core level orbitals. Li 1s spectra are magnified by a factor of 10 for clarity. XPS spectra of c) Li-BP and d) LiH-BP after exposing to the ambient for 1 h showing the formation of different phosphorous oxides. Insets: Surface crystallinity is tracked using LEED. The LEED pattern of Li-BP vanishes immediately upon exposure to the ambient, whereas that of LiH-BP remains stable.

without intercalation. Additionally, Li 1s core level peak shifts from 56.1 eV to 56.6 eV. The two different types of oxidation processes leading to the formation of P_4O_2 or P_2O_5 can be further distinguished by surface sensitive LEED. The formation of P_2O_5 (control sample) causes the LEED spots to be blurred, as shown in the inset of Figure 4c, which is consistent with the formation of a thicker oxidized phase. By contrast, the formation of P_4O_2 (LiH-BP sample) does not lead to degradation of surface crystallinity, as evidenced by the sharp LEED spots shown in the inset of Figure 4d, suggesting that these are just surface adsorbed oxygen. LiH is a good electron donor and can donate electrons to the electron trap sites in BP or can neutralize the hole oxidizers in BP, the latter is analogous to strategies used to counteract photocorrosion in common semiconductors,^[32] therefore the enhanced oxidation-resistance of LiH-BP can be due to the lowered chemical reactivity of BP following the passivation of oxygen-reactive defect sites by LiH.^[27,33] The relatively higher stability of LiH as compared to Li in the ambient is due to its much lower reactivity with N_2 and O_2 compared to Li.^[34]

BP has attracted much interest as a high mobility material with a decent on/off ratio, but its application in electronic device is hampered by poor stability. To date, the highest mobility for passivated BP field-effect transistors (FET) that do not use boron nitride encapsulation was reported to be $<100 \text{ cm}^2 \text{ V}^{-1} \text{ s}^{-1}$.^[10] To verify the robustness of the LiH intercalated BP, we tested the performance of FET devices as shown in Figure 5. All of the as-prepared devices show linear output characteristics (Figure 5a) of ohmic contact. Figure 5b,c shows

the transfer characteristics of both pristine BP and LiH-BP devices, respectively. As-prepared devices show ambipolar behavior with hole-dominated conduction and an on/off ratio of $\approx 10^3$. The field-effect mobilities ($\mu_{FE} = (1/C_{ox}) \times d\sigma/dV_{bg}$, where $C_{ox} = 12 \text{ nF cm}^{-2}$ is the back gate capacitance and σ is the channel conductivity) of both hole and electron for as-prepared devices in Figure 5c are estimated to be 646 and $14 \text{ cm}^2 \text{ V}^{-1} \text{ s}^{-1}$, respectively, consistent with previous reports. We note that Hall measurements generally give a mobility value smaller than the field effect mobility, in addition, the standard deviation of our measured values is one order of magnitude smaller than the average measured values.^[35] Remarkably, LiH-BP devices survived even after 18-day exposure in air (20°C , 56% humidity, natural indoor light illumination), and it maintained a high mobility of up to $\approx 800 \text{ cm}^2 \text{ V}^{-1} \text{ s}^{-1}$ and on/off ratio $>10^3$. By contrast, the pristine BP devices died after 2 d exposure. This striking contrast highlights the remarkable air-stability of our LiH-BP devices. However, it is worth noting that the air-exposed LiH-BP device showed a shift of the threshold voltages toward positive gate bias with increasing exposure time for both hole ($V_{th,p}$) and electron ($V_{th,n}$) conduction branches within the first half month (Figure S7, Supporting Information). We attribute this behavior to the p-doping effect from physisorbed oxygen and moisture on the channel surface, where there is a charge transfer of electrons from device channel to surface-absorbed O_2/H_2O species. This is consistent with our XPS results which show a decrease in P 2p core level binding energy by 0.25 eV, due to a p-doping induced Fermi

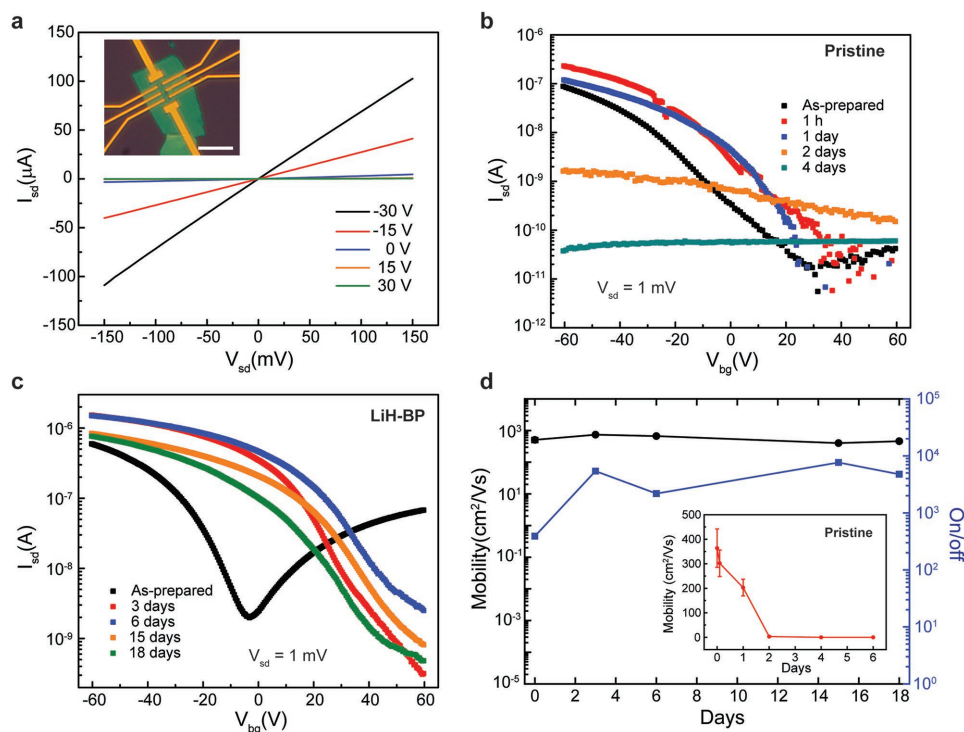


Figure 5. Transport properties of BP and LiH-BP after air exposure. a) Output curves of as-fabricated device. Inset shows an optical image of the corresponding device. Scale bar: 10 μm . Transfer characteristics of b) BP and c) LiH-BP devices for various ambient exposure times. d) Charge mobility and on/off ratio for LiH-BP as a function of air exposure time showing superior device stability for LiH-BP. Charge mobility for pristine BP as a function of exposure time is shown in the inset. Unintercalated BP devices failed after 2 d exposure to the ambient.

level shift toward the VB, shown in Figure 4. Additionally, the slight increase in mobility at the start of air exposure for LiH-BP devices is attributed to p-doping effect from ambient $\text{O}_2/\text{H}_2\text{O}$ species. Figure 5d shows the variation of hole mobility and on/off ratio with exposure time. Significantly, the carrier mobility of as-prepared LiH-BP remains comparable to unoxidized pristine BP, which reflects the negligible scattering effect from intercalated ions in the conduction channel. As shown in the inset, the mobility of the control BP devices decreases rapidly within 2 days, whereas LiH-BP devices show a relatively steady mobility value that decreases slowly with exposure time (9% decrease in mobility over a period of 18 days).

By chemically intercalating BP with LiH, we have shown that gap opening can be induced due to the decoupling of the near surface BP layers, along with improvement in chemical stability. Pseudo-monolayer LiH-BP ($x > 0.15$) with an optical gap of ≈ 1.7 eV and an electronic band gap of 1.98 eV (exciton binding energy ≈ 0.28 eV) can be generated on bulk BP. The increase in chemical stability can be attributed to the deactivation of oxygen-reactive defects in the near surface regions by LiH, thus limiting the oxidation rate. The passivation of electron trap sites by electron transfer from LiH imparts a high carrier mobility (≈ 800 $\text{cm}^2 \text{V}^{-1} \text{s}^{-1}$) on the FET device, while maintaining an on/off ratio of $>10^3$. The ability to fabricate stable BP devices allows the material to be exploited in optoelectronics and nanoelectronics. Finally, the LiH intercalation method, which is highly useful for generating quasi-monolayer on bulk 2D crystals, should be applicable to a wide class of 2D materials.

Experimental Section

Sample Preparation: The BP crystals used are single crystals purchased from HQGraphene. The BP samples were mounted onto a molybdenum sample plate and secured by two tantalum strips clamped at the two ends to the sample plate. The samples were peeled using a scotch-tape in situ to reveal a fresh surface before annealing in an ultrahigh vacuum chamber system of base pressure 4×10^{-10} Torr at 400 K for at least 2 h. Exfoliated nanosheets were transferred using a home-built HV transfer chamber after exfoliating in a nitrogen-filled glove box prior to loading into the ultra high vacuum (UHV) chamber in order to maintain pristine unoxidized surface of BP. Lithium was deposited onto the BP samples using commercial SAES Li getter source with the sample held at room temperature, typically at a rate of ≈ 0.3 ML h^{-1} . The flux was calibrated using XPS, and can be controlled using the current applied which regulates the temperature of the getter source. The source was thoroughly degassed before each deposition to minimize contamination. Intercalation was achieved by subsequent annealing at 400 K for 1 h. The hydrogenation reaction was carried out by annealing the sample in a chamber filled with 2×10^{-5} Torr of hydrogen at 450 K for around 1 h.

Sample Characterization: XPS characterizations were carried out using SPECS XR-50 X-ray Mg K α (1253.7 eV) source with a pass energy of 30 eV and a spot size of 5 mm. Detection is done by a PHOIBOS 150 hemispherical energy analyzer (SPECS, GmbH). The binding energies of the XPS spectra were calibrated using Au 4f $_{7/2}$ peaks. XPS peak fitting was carried out using a mixed Gaussian–Lorentzian function after a Shirley background subtraction. An area ratio of 2:1 between the P 2p $_{3/2}$ and 2p $_{1/2}$ peaks was employed in the fit with same FWHM. UPS measurements were performed with a monochromatized photon energy of 21.2 eV (He I) through a toroidal mirror monochromator (SPECS GmbH). The detector utilized is the same as XPS characterizations and the experiments were performed in a chamber of base pressure better

than 8×10^{-10} mbar. AFM measurements were performed with an XE-100 AFM 430 (Park Systems) under ambient conditions in noncontact mode with pointprobe plus-non-contact high resonance frequency reflex coating (PPP-NCHR) cantilevers purchased from Nanosensors. PL and Raman spectroscopy were performed using a WiTec Alpha 300R confocal Raman microscope with an excitation wavelength of 532 nm and a laser power of $<500 \mu\text{W}$. The laser was focused on the samples using 100 \times air-objective, and a spectral grating with 1800 lines mm^{-1} was used for all Raman spectra. LEED measurements were performed using ErLEED 1000A (SPECS, GmbH) at several positions on the BP crystals with a cathode current of 2.3 A, screen voltage of 5.0 kV, and electron energy of 179 V. Samples were annealed at 400 K for 2 h and allowed to cooldown to room temperature prior to measurements. HREELS measurements were performed using a Delta 0.5 spectrometer (SPECS, GmbH) in the coarse mode, specular armchair direction with an impinging electron energy of 16 eV. Energy resolution is 20 and 30 meV for pristine BP and LiH-BP, respectively.

Device Fabrication: Ultrathin BP nanosheets were mechanically exfoliated from bulk crystals (HQgraphene) and subsequently deposited onto silicon substrate with 285 nm thermal SiO_2 dielectric layer in an argon-filled glovebox. The thicknesses of the flakes were estimated by optical contrast. Electrode patterning was configured through electron beam lithography and following by deposition of Ti/Au (5 nm/70 nm) by thermal evaporation. After device fabrication, half of the devices were selected for Li intercalation and hydrogenation processes, and the other half was used for control experiment. Charge transport characterizations were carried out using a probe station in a nitrogen-filled glovebox.

Supporting Information

Supporting Information is available from the Wiley Online Library or from the author.

Acknowledgements

K.P.L. is grateful to the funding from the National Research Foundation, Prime Minister's Office, Mid-sized Research Centre (CA2DM). J.L. acknowledges the funding support from MOE-Tier 2 grant (R-143-000-682-112). I.A. acknowledges the NUS-Imperial Joint PhD program. The authors would like to thank Will Morrison, Dr. Thomas Albrecht, and Dr. Sung Park from Molecular Vista Inc. for their help with the PiFM measurements.

Conflict of Interest

The authors declare no conflict of interest.

Keywords

alkali metal intercalation, black phosphorus

Received: August 14, 2017

Revised: October 13, 2017

Published online:

- [1] H. B. Ribeiro, C. E. Villegas, D. A. Bahamon, D. Muraca, A. H. Castro Neto, E. A. de Souza, A. R. Rocha, M. A. Pimenta, C. J. de Matos, *Nat. Commun.* **2016**, *7*, 12191.
[2] J. Deng, Z. Chang, T. Zhao, X. Ding, J. Sun, J. Z. Liu, *J. Am. Chem. Soc.* **2016**, *138*, 4772.

- [3] a) J. Qiao, X. Kong, Z. X. Hu, F. Yang, W. Ji, *Nat. Commun.* **2014**, *5*, 4475; b) Z. Luo, J. Maassen, Y. Deng, Y. Du, R. P. Garrelts, M. S. Lundstrom, P. D. Ye, X. Xu, *Nat. Commun.* **2015**, *6*, 8572; c) X. Ling, S. Huang, E. H. Hasdeo, L. Liang, W. M. Parkin, Y. Tatsumi, A. R. Nugraha, A. A. Puzos, P. M. Das, B. G. Sumpter, D. B. Geohegan, J. Kong, R. Saito, M. Drndic, V. Meunier, M. S. Dresselhaus, *Nano Lett.* **2016**, *16*, 2260.
[4] Y. Cheng, Y. Zhu, Y. Han, Z. Liu, B. Yang, A. Nie, W. Huang, R. Shahbazian-Yassar, F. Mashayek, *Chem. Mater.* **2017**, *29*, 1350.
[5] J. Kim, S. S. Baik, S. H. Ryu, Y. Sohn, S. Park, B.-G. Park, J. Denlinger, Y. Yi, H. J. Choi, K. S. Kim, *Science* **2015**, *349*, 723.
[6] Z. Zhang, J. Waters, A. K. Geim, I. V. Grigorieva, *Nat. Commun.* **2017**, *8*, 15036.
[7] a) X.-f. Yu, H. Ushiyama, K. Yamashita, *Chem. Lett.* **2014**, *43*, 1940; b) A. Nie, Y. Cheng, S. Ning, T. Foroozan, P. Yasaei, W. Li, B. Song, Y. Yuan, L. Chen, A. Salehi-Khojin, F. Mashayek, R. Shahbazian-Yassar, *Nano Lett.* **2016**, *16*, 2240.
[8] W. Li, Y. Yang, G. Zhang, Y. W. Zhang, *Nano Lett.* **2015**, *15*, 1691.
[9] T. Eknapakul, P. D. King, M. Asakawa, P. Buaphet, R. H. He, S. K. Mo, H. Takagi, K. M. Shen, F. Baumberger, T. Sasagawa, S. Jungthawan, W. Meevasana, *Nano Lett.* **2014**, *14*, 1312.
[10] C. R. Ryder, J. D. Wood, S. A. Wells, Y. Yang, D. Jariwala, T. J. Marks, G. C. Schatz, M. C. Hersam, *Nat. Chem.* **2016**, *8*, 597.
[11] a) W. Luo, D. Y. Zemlyanov, C. A. Milligan, Y. Du, L. Yang, Y. Wu, P. D. Ye, *Nanotechnology* **2016**, *27*, 434002; b) S. Walia, Y. Sabri, T. Ahmed, M. R. Field, R. Ramanathan, A. Arash, S. K. Bhargava, S. Sriram, M. Bhaskaran, V. Bansal, S. Balendhran, *2D Mater.* **2016**, *4*, 015025.
[12] a) J.-S. Kim, Y. Liu, W. Zhu, S. Kim, D. Wu, L. Tao, A. Dodabalapur, K. Lai, D. Akinwande, *Sci. Rep.* **2015**, *5*, 8989; b) S. Das, M. Demarteau, A. Roelofs, *ACS Nano* **2014**, *8*, 11730; c) J. Na, Y. T. Lee, J. A. Lim, D. K. Hwang, G.-T. Kim, W. K. Choi, Y.-W. Song, *ACS Nano* **2014**, *8*, 11753.
[13] J. D. Wood, S. A. Wells, D. Jariwala, K.-S. Chen, E. Cho, V. K. Sangwan, X. Liu, L. J. Lauhon, T. J. Marks, M. C. Hersam, *Nano Lett.* **2014**, *14*, 6964.
[14] a) X. Chen, Y. Wu, Z. Wu, Y. Han, S. Xu, L. Wang, W. Ye, T. Han, Y. He, Y. Cai, N. Wang, *Nat. Commun.* **2015**, *6*, 7315; b) Y. Cao, A. Mishchenko, G. L. Yu, E. Khestanova, A. P. Rooney, E. Prestat, A. V. Kretinin, P. Blake, M. B. Shalom, C. Woods, J. Chapman, G. Balakrishnan, I. V. Grigorieva, K. S. Novoselov, B. A. Piot, M. Potemski, K. Watanabe, T. Taniguchi, S. J. Haigh, A. K. Geim, R. V. Gorbachev, *Nano Lett.* **2015**, *15*, 4914; c) A. Avsar, I. J. Vera-Marun, J. Y. Tan, K. Watanabe, T. Taniguchi, A. H. Castro Neto, B. Özyilmaz, *ACS Nano* **2015**, *9*, 4138.
[15] J. Pei, X. Gai, J. Yang, X. Wang, Z. Yu, D. Y. Choi, B. Luther-Davies, Y. Lu, *Nat. Commun.* **2016**, *7*, 10450.
[16] Q. Li, Q. Zhou, X. Niu, Y. Zhao, Q. Chen, J. Wang, *J. Phys. Chem. Lett.* **2016**, *7*, 4540.
[17] a) S. Sugai, I. Shirovani, *Solid State Commun.* **1985**, *53*, 753; b) Y. Akahama, M. Kobayashi, H. Kawamura, *Solid State Commun.* **1997**, *104*, 311.
[18] a) R. Fei, L. Yang, *Appl. Phys. Lett.* **2014**, *105*, 083120; b) Y. Wang, C. Cong, C. Qiu, T. Yu, *Small* **2013**, *9*, 2857; c) B. Chakraborty, A. Bera, D. V. S. Muthu, S. Bhowmick, U. V. Waghmare, A. K. Sood, *Phys. Rev. B* **2012**, *85*, 161403; d) Y. Wang, C. Cong, R. Fei, W. Yang, Y. Chen, B. Cao, L. Yang, T. Yu, *Nano Res.* **2015**, *8*, 3944.
[19] C. Pepin, P. Loubeyre, F. Occelli, P. Dumas, *Proc. Natl. Acad. Sci. USA* **2015**, *112*, 7673.
[20] A. Lazicki, P. Loubeyre, F. Occelli, R. J. Hemley, M. Mezour, *Phys. Rev. B* **2012**, *85*, 054103.
[21] a) I. Alexandrou, K. Chremmou, A. J. Papworth, U. Bangert, G. A. J. Amaratunga, C. J. Kiely, *Diamond Relat. Mater.* **2005**, *14*, 1522; b) M. Vos, S. W. King, B. L. French, *J. Electron Spectrosc. Relat. Phenom.* **2016**, *212*, 74.

- [22] Y. Liu, Z. Qiu, A. Carvalho, Y. Bao, H. Xu, S. J. Tan, W. Liu, A. H. Castro Neto, K. P. Loh, J. Lu, *Nano Lett.* **2017**, *17*, 1970.
- [23] L. Li, J. Kim, C. Jin, G. J. Ye, D. Y. Qiu, F. H. da Jornada, Z. Shi, L. Chen, Z. Zhang, F. Yang, K. Watanabe, T. Taniguchi, W. Ren, S. G. Louie, X. H. Chen, Y. Zhang, F. Wang, *Nat. Nanotechnol.* **2017**, *12*, 21.
- [24] a) V. Tran, R. Soklaski, Y. Liang, L. Yang, *Phys. Rev. B* **2014**, *89*, 235319; b) L. Liang, J. Wang, W. Lin, B. G. Sumpter, V. Meunier, M. Pan, *Nano Lett.* **2014**, *14*, 6400.
- [25] X. Wang, A. M. Jones, K. L. Seyler, V. Tran, Y. Jia, H. Zhao, H. Wang, L. Yang, X. Xu, F. Xia, *Nat. Nanotechnol.* **2015**, *10*, 517.
- [26] R. Xu, S. Zhang, F. Wang, J. Yang, Z. Wang, J. Pei, Y. W. Myint, B. Xing, Z. Yu, L. Fu, Q. Qin, Y. Lu, *ACS Nano* **2016**, *10*, 2046.
- [27] D. Xiang, C. Han, J. Wu, S. Zhong, Y. Liu, J. Lin, X. A. Zhang, W. Ping Hu, B. Özyilmaz, A. H. Neto, A. T. Wee, W. Chen, *Nat. Commun.* **2015**, *6*, 6485.
- [28] A. Favron, E. Gaufres, F. Fossard, A. L. Phaneuf-L'Heureux, N. Y. Tang, P. L. Levesque, A. Loiseau, R. Leonelli, S. Francoeur, R. Martel, *Nat. Mater.* **2015**, *14*, 826.
- [29] a) S. P. Koenig, R. A. Doganov, H. Schmidt, A. H. C. Neto, B. Özyilmaz, *Appl. Phys. Lett.* **2014**, *104*, 103106; b) C.-G. Andres, V. Leonardo, P. Elsa, O. I. Joshua, K. L. Narasimha-Acharya, I. B. Sofya, J. G. Dirk, B. Michele, A. S. Gary, J. V. Alvarez, W. Z. Henny, J. J. Palacios, S. J. v. d. Z. Herre, *2D Mater.* **2014**, *1*, 025001.
- [30] M. T. Edmonds, A. Tadich, A. Carvalho, A. Ziletti, K. M. O'Donnell, S. P. Koenig, D. F. Coker, B. Özyilmaz, A. H. Neto, M. S. Fuhrer, *ACS Appl. Mater. Interfaces* **2015**, *7*, 14557.
- [31] A. Ziletti, A. Carvalho, P. E. Trevisanutto, D. K. Campbell, D. F. Coker, A. H. Castro Neto, *Phys. Rev. B* **2015**, *91*, 085407.
- [32] a) E. Kooi, *The Surface Properties of Oxidized Silicon*, Springer, Berlin **1967**; b) B. Gokce, D. B. Dougherty, K. Gundogdu, *J. Vac. Sci. Technol., A* **2012**, *30*, 040603; c) C. L. Hinkle, A. M. Sonnet, M. Milojevic, F. S. Aguirre-Tostado, H. C. Kim, J. Kim, R. M. Wallace, E. M. Vogel, *Appl. Phys. Lett.* **2008**, *93*, 113506.
- [33] S. Ghosh, G. G. Khan, A. Ghosh, S. Varma, K. Mandal, *CrystEngComm* **2013**, *15*, 7748.
- [34] S. J. Tan, I. Abdelwahab, Z. Ding, X. Zhao, T. Yang, G. Z. Loke, H. Lin, I. Verzhbitskiy, S. M. Poh, H. Xu, C. T. Nai, W. Zhou, G. Eda, B. Jia, K. P. Loh, *J. Am. Chem. Soc.* **2017**, *139*, 2504.
- [35] a) B. W. H. Baugher, H. O. H. Churchill, Y. Yang, P. Jarillo-Herrero, *Nano Lett.* **2013**, *13*, 4212; b) L. Li, Y. Yu, G. J. Ye, Q. Ge, X. Ou, H. Wu, D. Feng, X. H. Chen, Y. Zhang, *Nat. Nanotechnol.* **2014**, *9*, 372.